Electronic Supplementary Material (ESI) for Nanoscale.
This journal is © The Royal Society of Chemistry 2020

Electronic Supplementary Information for:

Understanding the structural diversity of freestanding Al_2O_3 ultrathin films through a DFTB-aided genetic algorithm

Maxime Van den Bossche, Claudine Noguera, and Jacek Goniakowski

CNRS and Sorbonne Université, Institut des NanoSciences de Paris, UMR 7588, 4 Place Jussieu, F-75005 Paris, France

Contents

1 Genetic operators in the 2D-GA

The different genetic operators used in the 2D-GA are listed in Table 1. These can be seen as the 2D equivalents of 3D operators used in crystal structure optimization.[1,2,3]

Table 1

Operator	Probability	Description
Cut-and-splice pairing	50%	Cuts two parent structures along a plane perpendicular to a randomly chosen cell vector and combines the different halves into a new structure. The new **a** and **b** vectors are chosen as random linear combinations of the parent vectors and are then rescaled so that the initial surface area corresponds to the average of the best 20% structures in the population.
Strain mutation	15%	Scales the surface unit cell vectors and atomic positions according to strain components drawn from a Gaussian distribution with $\sigma = 0.7$.
Shear mutation	10%	Applies a shear strain perpendicular to the **a** or **b** vectors (chosen at random), which hence only affects the atomic c coordinates.
Rattle mutation	10%	Randomly displaces 80% of the atomic coordinates with amplitudes uniformly selected between 0 and 2.5 Å.
Soft mutation	15%	Moves the atoms along the vibrational mode with the lowest frequency, as identified by a simple pairwise interaction model.[4] If a structure has already been soft mutated, the next vibrational mode is chosen.

2 Bulk energetics with the `matsci` DFTB parameters

Table 2 shows the relative energies (per formula unit) for various bulk Al_2O_3 polytypes calculated with the present DFT setup and with the `matsci`[5] DFTB parameter set using ℓ-dependent Hubbard parameters. Bulk Al_2O_3 polymorphism was not taken into account in the `matsci` parametrization procedure, leading to a poor description of the energetical ordering.

Table 2

		ΔE (eV/f.u.)	
	Model	optB86b -vdW	DFTB `matsci`[5]
α		0	0
θ		0.15	-0.56
κ		0.15	-0.31
γ	γ_{MG}[6]	0.30	-0.52
	γ_{PN}[7]	0.30	-0.52
	γ_{PR}[8,9]	0.42	0.16
	γ_{KR}[10]	0.23	-0.02
δ	δ_{RH}[11]	0.43	-0.23
	δ_{KB1}[12]	0.14	-0.50
	δ_{KB2}[12]	0.14	-0.50
bixbyite		0.17	-0.58

3 Structures of known bulk polymorphs

Figure 1: Structures of the known bulk polymorphs listed in Table 1 of the main text and in Table 2 of the ESI. The atomic coordinates and cell vectors are provided in the ZIP archive of the ESI.

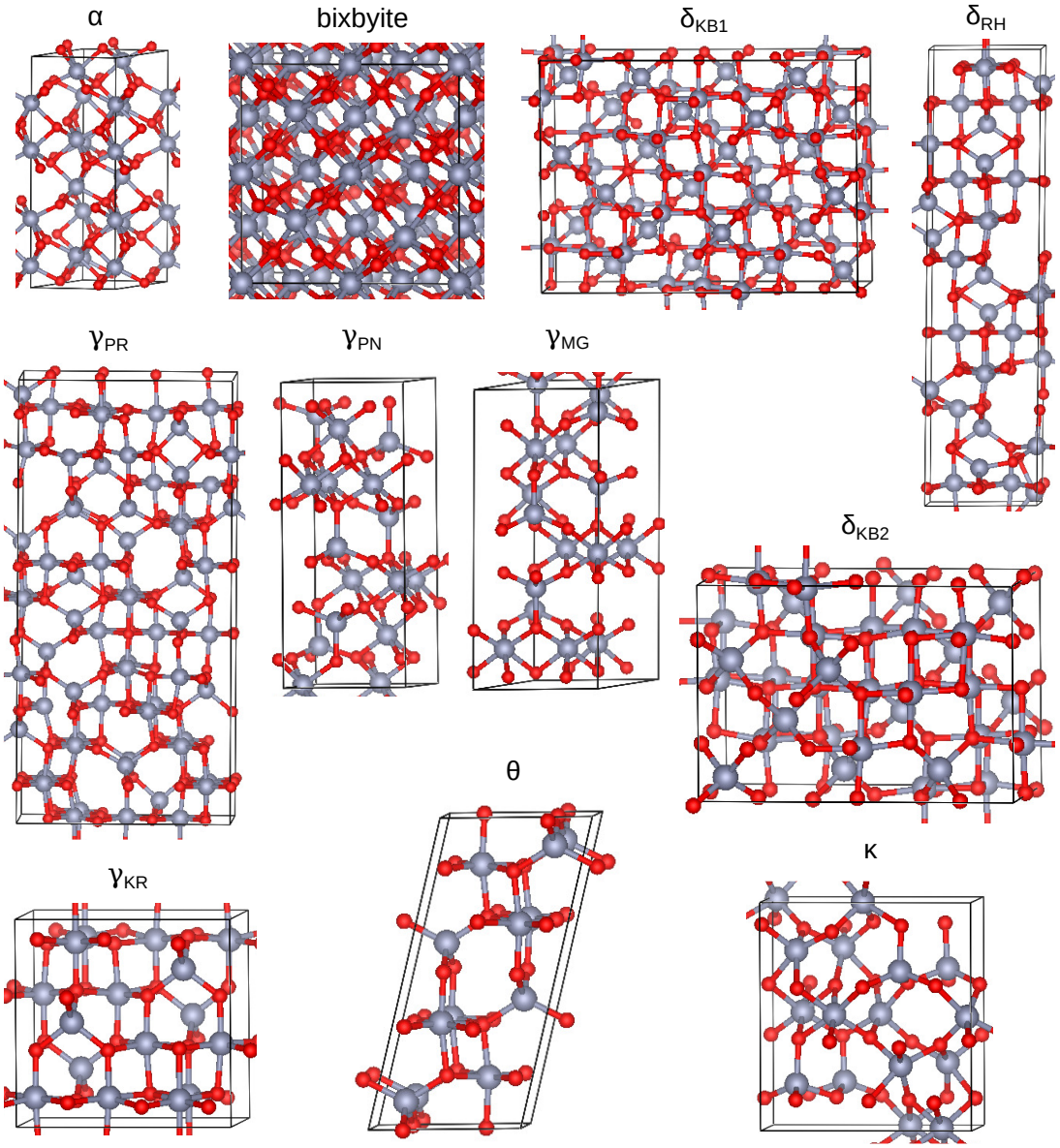

4 Parity diagrams for the thin film training set

Figures 2 and 3 show the parity diagrams for the `bulk-opt` (blue) and `film-opt` (orange) DFTB total energies for two series of Al_2O_3 thin films, in comparison with DFT. The thin film structures have been obtained by 2D-GA searches in the thickness intervals of 3.5-5 Å (Figure 2) and 6.5-8 Å (Figure 3) using the `bulk-opt` parametrization. The `film-opt` parameters have been refined so as to minimize the deviation from parity for these data sets.

Figure 2: 3.5-5 Å thickness interval.

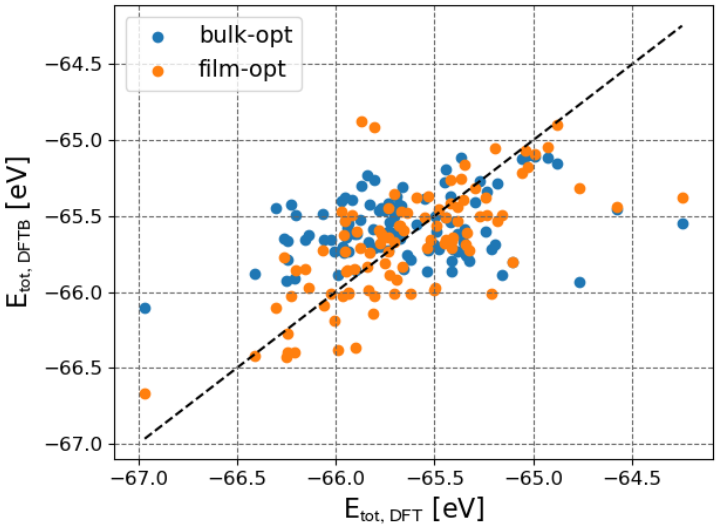

Figure 3: 6.5-8 Å thickness interval.

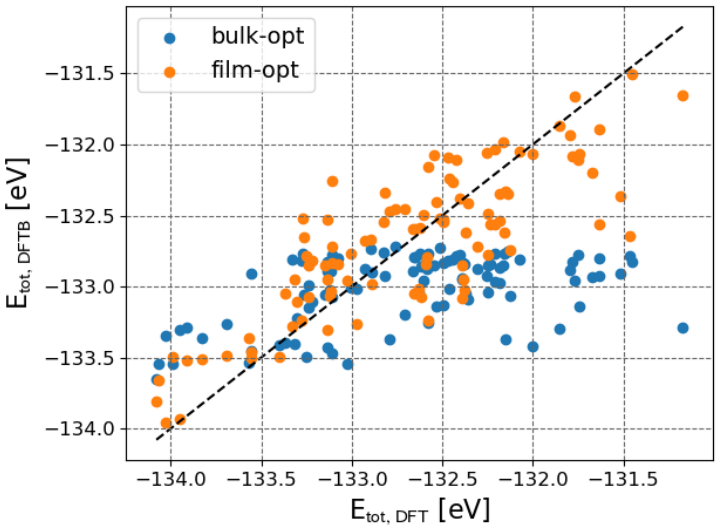

5 Structure-stability relations in bulk Al_2O_3

To illustrate the difficulties in relating the relative stabilities of the bulk Al_2O_3 polymorphs to differences in local bonding patterns, we analyze the variation in cation coordination as well as a model based on correlations between bond strengths and bond lengths.

5.1 Cation coordination

The abundances of four- and six-fold coordinated Al atoms for different known bulk polymorphs are listed in Table 3 together with energy differences calculated with DFT. The lack of correlation between both properties can be appreciated by considering e.g. the most stable α polymorph where all Al atoms are six-fold coordinated. Assigning a higher stability to this local environment, however, would be contradicted by the relative instability of the bixbyite phase (consisting also exclusively of 6-fold Al) compared to several other phases with significant concentrations of 4-fold Al atoms (i.e. κ, θ, δ_{KB1} and δ_{KB2}).

5.2 Bond-length-bond-strength correlation

The relative stabilities of different bulk structures may also be assessed in terms of the number and strength of the Al-O bonds. A commonly applied expression for bond strengths using only local geometric information is given by the model of Pauling[13] and Brown and coworkers[14]:

$$E_{\mathrm{bond}}(r) = \exp\left(\frac{r - r_0}{b}\right), \tag{1}$$

with parameters b and r_0. Energy differences per formula unit may then be written as:

$$\Delta E_{\mathrm{A-B}} = \left(\sum_{\mathrm{Al-O\ \ bonds}} E_{\mathrm{bond}}(r_{\mathrm{Al-O}})/N_{\mathrm{f.u.}}\right)_A - \left(\sum_{\mathrm{Al-O\ \ bonds}} E_{\mathrm{bond}}(r_{\mathrm{Al-O}})/N_{\mathrm{f.u.}}\right)_B . \tag{2}$$

The last column in Table 3 shows the performance of such a model where r_0 and b have been adjusted to reproduce the DFT energy differences w.r.t. α-Al_2O_3 via least-squares fitting. The fitted parameter values are $r_0 = 2.29$ Å and $b = 0.35$ Å. While the model retrieves α-Al_2O_3 as the most stable polymorph, it is clear that also this approach is not sufficiently accurate for the present purposes.

Table 3

Model	Al coordination		ΔE (eV/f.u.)	
	4-fold (%)	6-fold (%)	optB86b -vdW	Bond model
α	0	100	0	0
δ_{KB1}[12]	38	62	0.14	0.27
δ_{KB2}[12]	38	62	0.14	0.29
θ	50	50	0.15	0.51
κ	25	75	0.15	0.34
bixbyite	0	100	0.17	0.57
γ_{KR}[10]	25	75	0.23	0.19
γ_{MG}[6]	38	62	0.30	0.40
γ_{PN}[7]	38	62	0.30	0.41
γ_{PR}[8,9]	33	67	0.42	0.43
δ_{RH}[11]	38	62	0.43	0.69

6 Vacancy refilling on $\delta_{KB1}(100)$ and $\delta_{KB2}(100)$

Figures 4 and 5 show the displacements of low-coordinated Al atoms into surface cation vacancies on $\delta_{KB1}(100)$ and $\delta_{KB2}(100)$. The displacements for $\gamma_{MG}(001)$ are shown in Figure 7 in the main text.

Figure 4: $\delta_{KB1}(100)$

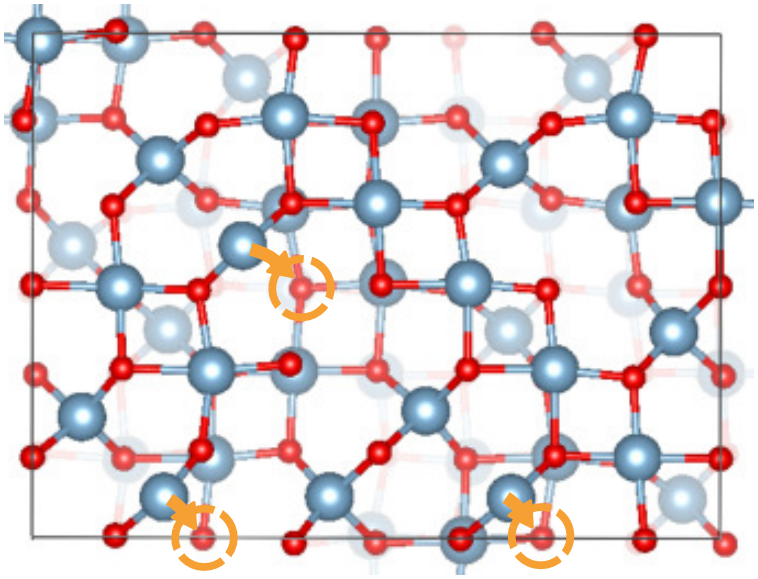

Figure 5: $\delta_{KB2}(100)$

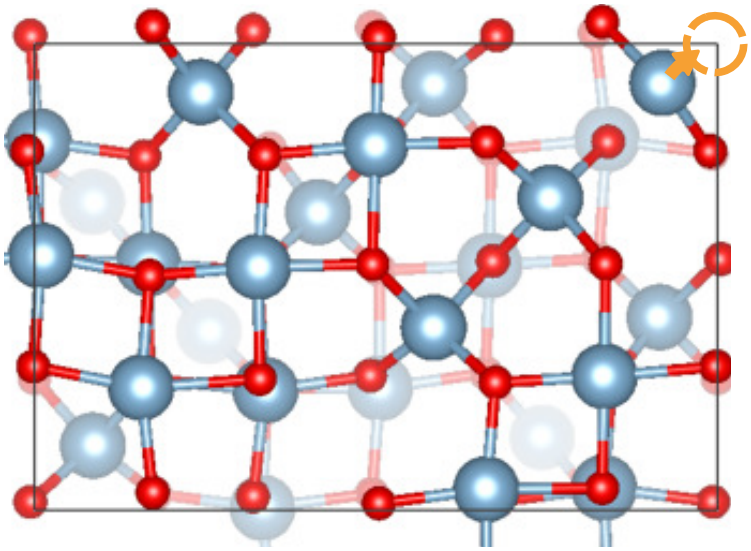

References

[1] C. W. Glass, A. R. Oganov, and N. Hansen. *Comput. Phys. Commun.* **175**, 11-12 (2006), 713–720.

[2] D. C. Lonie and E. Zurek. *Comput. Phys. Commun.* **182**, 2 (2011), 372–387.

[3] M. Van den Bossche, H. Grönbeck, and B. Hammer. *J. Chem. Theory Comput.* **14**, 5 (2018), 2797–2807.

[4] A. O. Lyakhov, A. R. Oganov, and M. Valle. *Comput. Phys. Commun.* **181**, 9 (2010), 1623–1632.

[5] J. Frenzel et al. *Z. Anorg. Allg. Chem.* **631**, 6-7 (2005), 1267–1271.

[6] E. Menéndez-Proupin and G. Gutiérrez. *Phys. Rev. B* **72**, 3 (2005), 035116.

[7] H. P. Pinto, R. M. Nieminen, and S. D. Elliott. *Phys. Rev. B* **70**, 12 (2004), 125402.

[8] G. Paglia et al. *Phys. Rev. B* **71**, 22 (2005), 224115.

[9] G. Paglia et al. *Phys. Rev. B* **68**, 14 (2003), 144110.

[10] X. Krokidis et al. *J. Phys. Chem. B* **105**, 22 (2001), 5121–5130.

[11] Y. Repelin and E. Husson. *Mat. Res. Bull.* **25**, 5 (1990), 611–621.

[12] L. Kovarik et al. *J. Phys. Chem. C* **118**, 31 (2014), 18051–18058.

[13] L. Pauling. *J. Am. Chem. Soc.* **69**, 3 (1947), 542–553.

[14] I. D. Brown and R. D. Shannon. *Acta Cryst. A* **29**, 3 (1973), 266–282.